J. S. Afr. Inst. Min. Metall., vol. 91, no. 4.
Apr. 1991. pp. 137-144.

The propagation of shock waves in a complex tunnel system

by B.W. SKEWS* and W.R. LAW*

SYNOPSIS

This paper describes an investigation into the behaviour of a shock wave propagating through a system of branched ducts such as can occur in an underground mining complex after an explosion. A simple numerical model that predicts flow properties within the ducts was evaluated by use of pressure measurements and schlieren photography of the transient flow within the ducts. The results returned by the model compared well with the measured values, and verified the model's ability to provide an approximate estimate of shock-wave behaviour in propagation problems of this type. The experimental results revealed the establishment of complex flow patterns in the ducts after the arrival of the incident shock wave. The average pressure inside the test section rose to approximately double the pressure behind the incident shock. This pressure acts as a source to drive shock waves into other sections of the duct system. It is shown that the series of shock waves emerging from the test section into an adjacent tunnel coalesce to form an even stronger wave, and that the attenuation of the wave through this typical tunnel geometry is surprisingly small.

SAMEVATTING

Hierdie referaat beskryf 'n ondersoek na die gedrag van 'n skokgolf wat in 'n stelsel van vertakte tonnels voortgeplant word, soos kan gebeur in 'n ondergrondse myn kompleks as gevolg van 'n ontploffing. 'n Eenvoudige numeriese model om die vloei-eienskappe binne die tonnels te voorspel is geëvalueer deur van drukmeting en schlieren-fotografie van die vloei in die tonnels gebruik te maak. Die resultate wat d.m.v. die numeriese model verkry is, het gunstig vergelyk met die waardes wat deur meting verkry is en het bewys dat die model oor die vermoë beskik om 'n aanduiding te gee van die gedrag van skokgolwe wanneer hulle voortgeplant word, in situasies van hierdie soort. Die eksperiment se resultate het die ontstaan van komplekse vloeipatrone in die tonnels na die aankoms van die invalskok getoon. Die gemiddelde druk in die toetssegment het tot ongeveer dubbel die druk agter hierdie invalskok gestyg. Hierdie druk het die gevolg dat skokgolwe in ander dele van die tonnelstelsel ingedryf word. Die skokgolwe kombineer om 'n sterker golf te vorm, en die verswakking van die skokgolf in so 'n tipiese tonnelsisteem is verbasend klein.

Introduction

Knowledge about the behaviour of shocks in branched ducts has important applications in many engineering fields, including the transmission of oil and gas in pipelines, the inlets and exhausts of reciprocating machines, the design of buildings in which to store explosives and, conversely, the design of structures to protect people from explosions. In the mining industry, the study of the behaviour of shock waves in a system of branched ducts can serve as a basis for the prediction and control of explosive fronts in mine tunnels. The geometry of a tunnel system can be a dominant factor in determining the magnitude of the pressure increase associated with an underground explosion.

In 1959, at the President Steyn Gold Mine, such an accidental explosion caused a strong shock wave to move down the main haulage towards a stope and its series of cross-cuts[1]. The inter-connecting tunnel system at the end of the haulage is indicated in Fig. 1. The severity of the damage caused by this blast on either side of this system suggested unexpected behaviour by the shock waves in negotiating corners, branches, and dead ends.

The experimental test section used in the work described in the present paper was an idealized geometric model of the portion of the mine referred to above. The investigation was a direct attempt to get an understanding, both by experiment and through numerical modelling, of the behaviour of shock waves as they move through such a tunnel system. It is a simplified model and does not attempt to reproduce all the factors involved in the original accident. It does not, for example, take account of blast propagation across the interconnecting cross-cuts between the haulage and the return airway, situated to the left of the system shown in Fig. 1.

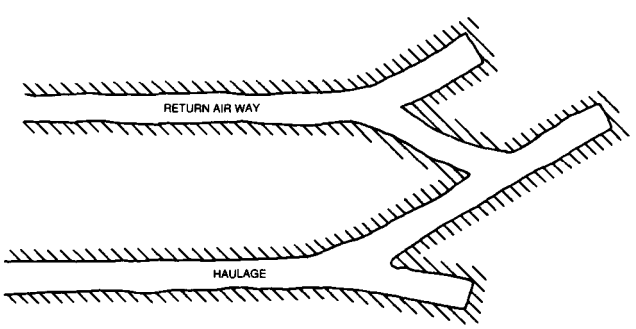

Fig. 1—The geometry of the mine tunnel

The objects of the investigation were two-fold: firstly, using schlieren photography and high-speed pressure measurement, to investigate the behaviour of a shock wave propagating through a system of branched ducts and, secondly, to evaluate an approximate numerical model to predict shock-wave Mach numbers, from which pressures, temperatures, and gas velocities within the system boundaries can be calculated.

* University of the Witwatersrand, P.O. Wits, Transvaal.

ISSN 0038-223X/3.00 + 0.00. Paper received 4th September, 1990.

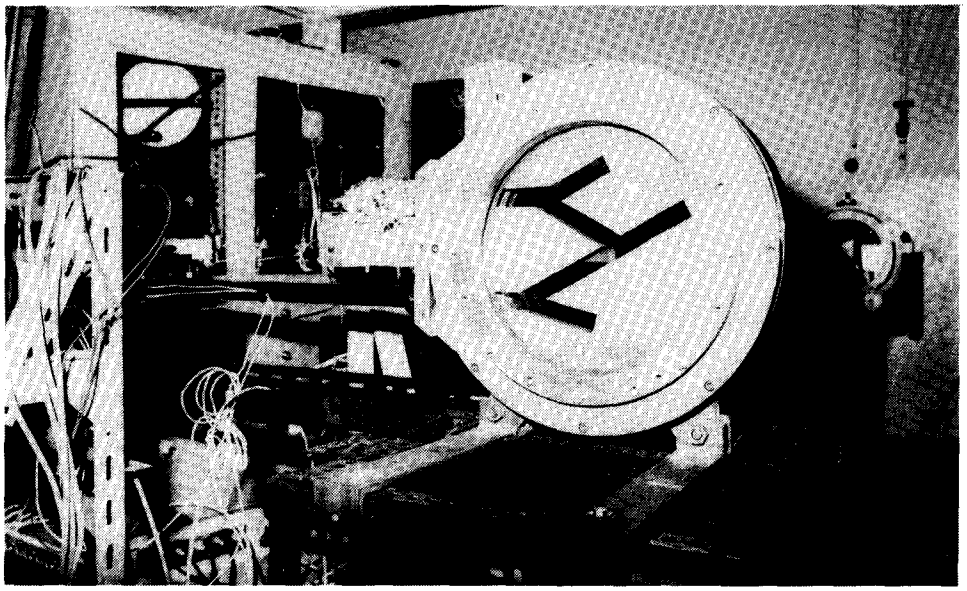

Fig. 2—The test section installed at the end of the shock tube

Equipment

The basic requirements of the laboratory apparatus were to generate a shock wave under controlled conditions, and to feed it into the test section, where its strength could be measured at several locations. Schlieren photographs of the shock profiles and other flow phenomena were also required. A plane incident wave with uniform flow behind it was desirable, so that all the transverse waves and two-dimensional effects observed were a consequence of the system of branches and were not confounded by waves that could arise further upstream.

A conventional shock tube was designed and built to generate the shock wave. The tube was 6 m long (a driver section 1 m in length and an expansion section of 5 m), and had a constant square cross-section of 20 by 20 mm. Separating these two sections was a thin diaphragm made from cellulose acetate sheet. The driver section could be pressurized to 1,5 MPa. The expansion section remained at atmospheric pressure (approximately 87 kPa). Diaphragm bursting was accomplished through a natural pressure burst or electrically. This latter method involved painting a 'bow tie'-shaped pattern on the surface of the diaphragm with conductive spray paint. The diaphragm was then installed in such a way that a suitable voltage could be switched across it. The maximum resistance at the centre of the pattern caused a small hole to be burnt in the centre of the diaphragm once the switch had been closed. The diaphragm, which was highly pressurized at that stage, shattered, resulting in a plane shock wave moving down the expansion section.

The test section, or model, consisted essentially of a vertically mounted cylindrical 'slice' of mild steel, of diameter 300 mm, into which the ducts (20 by 20 mm in cross-section) had been machined. It could be used in two modes: in pressure measurement, for which a pressure plate containing transducers was mounted on one side with the other side blanked off, and in schlieren photography, where optically clear glass plates were mounted on both sides. Fig. 2 shows the test section, in schlieren mode, installed at the end of the shock tube. For the pressure measurement, two transducers (PCB 113A21) were mounted in ports along the expansion section of the tube, and another five in ports on the pressure plate positioned to coincide with points of interest in the ducts. The transducers were linked to a computer-based data-acquisition system, which allowed pressure–time data to be recorded and analysed.

Schlieren photography was achieved by use of an argon-jet light source, with a flash of 0,3 μs duration linked to a delay unit calibrated in microseconds and triggered by one of the transducers mounted in the expansion section of the shock tube. Two 250 mm parabolic mirrors and a knife-edge and lens system produced the schlieren effect, which was recorded either on positive/negative Polaroid instant film or 35 mm colour film. The optical density of a schlieren image is proportional to the density gradients within the gas, and is thus an ideal method for the visualization of compressible gas dynamic phenomena.

Theory

The theory is based on a method proposed by Heilig[2] for analysing shock movement through branched ducts, extended to cases with non-symmetric and obtusely angled branches. It is an approximate method that is being evaluated in parallel with high-resolution numerical schemes, which are comparatively expensive in computer time and are not reported on here.

The aim of the method is to predict, independently from experimental data, the intensity of the shocks in the branches of a junction as a function of the intensity of the incident shock and geometry of the junction. The procedure is illustrated below for a simple 45° junction as shown in Fig. 3, and can be summarized as follows.

(1) The shape of the diffracted shock at the instant when it reaches apex R can be calculated by Whitham's theory[3] of shock dynamics.
(2) The assumption is then made that the flux of energy owing to a curved part-shock spanning the inlet to a branch is the same as that for when the part-shock has smoothed out into a plane shock in the branch.

Whitham's theory is an approximate treatment that gives information on the shape of the diffracting shock.

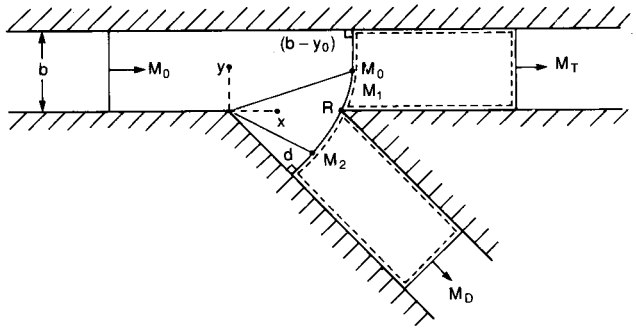

Fig. 3—An example to show the application of Heilig's method

The shock positions at different times and the orthogonal trajectories of this set, termed *rays*, form an orthogonal mesh. The propagation of the shock between two neighbouring rays can be treated as if the rays were solid walls, i.e. the ray tubes are regarded as channels. Chester and Chisnell[4] developed a 'channel formula', given by $A = A(M)$, in which the cross-sectional area A is a decreasing function of the Mach number M of the shock moving down the channel. Whitham's theory does not treat the afterflow region of the diffracted shock wave since the particles can be considered to follow a ray only in the neighbourhood of the moving shock wave. It also ignores the effect of this perturbed region on the diffration geometry. The accuracy of the method has been evaluated by Skews[5].

For the present illustrative case (Fig. 4), Whitham's theory enables the goemetry of the shock diffracted around the inlet corner L of the junction to be calculated at a fixed time for a given primary mach number, M_0 and a corner angle, γ. In this diffraction process with $\gamma = 45°$, a simple wave originating at L spreads out on the plane shock and causes its curvature between P_0 and P_2. The angle Θ of a ray with the x-axis decreases in the fan from zero at P_0 to a negative final value at its end P_2. Likewise, the shock mach number, M, decreases from M_0 at P_0 to M_2 at P_2. The diffracted shock leaving the fan at P_2 is plane and meets the wall perpendicularly. For all M_0, the last characteristic, LP_2, never reaches the wall, i.e. the expansion fan ends within the flow field. The first characteristic, LP_0, is inclined to the x-axis at angles not greater than 23,9° for all primary shock-wave intensities.

After transformation onto Cartesian coordinates, the

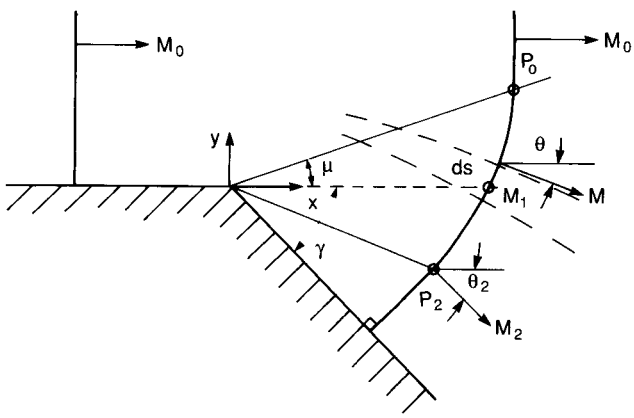

Fig. 4—Diffraction of a plane shock wave around a corner

angle Θ of ray inclination is related to the shock Mach number by the integral

$$\Theta(M) = \int_{M_0}^{M} \frac{dM}{W(M)}, \quad \ldots\ldots (1)$$

where $W(M)$ is obtained from

$$W(M) = \sqrt{0{,}5 \times (M^2 - 1) \times K(M)}. \quad \ldots\ldots (2)$$

$K(M)$ is the Chester function, and comes from the Chester–Chisnell channel formula,

$$K(M) = 2 \times \left[\left(1 + \frac{2}{k+1} \times \frac{1-\mu^2}{\mu}\right)(2 \times \mu + 1 + M^{-2})\right]^{-1}, \quad \ldots\ldots (3)$$

where the variable μ is defined by

$$\mu^2 = \frac{(k-1) \times M^2 + 2}{2 \times k \times M^2 - (k-1)}, \quad \ldots\ldots (4)$$

and k is the ratio of specific heats. The slope $\mu(M)$ of each characteristic in the linear characteristic fan (this μ is different from the μ used by Chester) is given by

$$\mu(M) = \tan[\Theta(M) + m(M)], \quad \ldots\ldots (5)$$

where $m(M) = \arctan\left[\frac{1}{M} \times W(M)\right]$ ..... (6)

The value $m(M)$ is analogous to the Mach angle in steady supersonic flow. With the line element $ds(M)$ between two rays, the equations for the space variables x and y of the shock at time t are

$$dx = -\sin\Theta \times ds \quad \ldots\ldots (7)$$

and

$$dy = \cos\Theta \times ds. \quad \ldots\ldots (8)$$

Finally, the initial values are

$$x_0 = M_0 \times \alpha$$

and

$$y_0 = \mu(M_0) \times M_0 \times \alpha.$$

The factor proportional to time, α, indicates that the shapes of the diffracted wavefronts at different times are geometrically similar with L as centre. The integration of equations (1), (2), (7), and (8) for a specific primary Mach number and wall angle can then be performed. The value M_1 comes from $\mu(M_1) = 0$, and M_2 from $\Theta(M_2) = -\gamma$. These geometric 'boundary conditions', as they can be called, will differ from every junction geometry.

The second item in the theory mentioned above is that related to energy conservation. As shown in Fig. 3, the diffracted shock splits up into two part-shocks, each of which enters its own branch. The part-shock wave is assumed to smooth out and become plane. (This does occur in practice through the mechanism of multiple Mach reflections.) It is further assumed that the energy flux of a part-shock is equal to that of its smoothed out state. In Mach reflection, part of the reflected shock wave overtakes the initial shock wave from behind, its energy being added back to the wave.

Nevertheless, there are several energy losses not

included in the assumption based on an ideal gas, e.g. the energy lost by wall friction, heat conduction, or real gas effects. Also directly neglected in the approximation is the energy of the part of the reflected shock that moves away from the initial shock, the energy associated with the expansion wave moving upstream, and the energy of any secondary shocks in the branches. It is assumed that their energy fluxes should be low compared with that of the dominant transmitted and deflected shocks. For a two-dimensional junction with depth τ and using Rankine–Hugoniot's equations with 1,4 as the ratio of specific heats, the energy assumption mentioned above yields the term[2]

$$E(M) = \frac{35}{6} \times \left(M^3 - 4 \times M + \frac{18 \times M}{M^2 + 5} \right) \times s \times \tau. \quad (9)$$

M is the Mach number on a part of the shock with length s, while $E(M)$ is the energy increase in unit time normalized by the velocity of sound and the pressure ahead of the shock. That it holds true is the main assumption on which this numerical method is based.

With reference to Fig. 3, the following conservation equations hold in the main branch of the junction and in the side branch respectively:

$$\int_{M_1}^{M_0} E(M) \times ds + E(M_0) \times (b - y_0) = E(M_T) \times b \quad (10)$$

$$\int_{M_2}^{M_1} E(M) \times ds + E(M_2) \times d = E(M_D) \times b, \ldots\ldots \quad (11)$$

where $b = x_1 \times \sin \gamma$

$$d = |y_2 - x_2| / \sqrt{2} \text{ for } \gamma = 45°.$$

The plane portions of the total diffracted shock with the lengths $b - y_0$ and d were described above in connection with the expansion fan. Equations (10) and (11) are then solved for M_T and M_D, these being the shock Mach numbers of the smoothed-out deflected shock in the main branch and the side branch respectively.

Based on this theoretical concept, all the junctions in the mine test section could be analysed. All that varies are the boundary conditions relating to the particular geometry of each branch.

Results and Discussion

Figs. 5 to 8 show schlieren photographs of the flow as the shock-wave system propagates through the various ducts. These photographs were taken for an incident shock wave with a Mach number of 1,38. The time interval between the pictures is approximately 32 μs.

Fig. 5a is the shape of the wave predicted by Whitham's theory, and Fig. 5b is the corresponding schlieren photograph. The correlation between the predicted shock geometry and that obtained experimentally is good. Also visible in the photograph (and neglected by the theory) are two expansion waves that emanate from each of the corners. As the flow behind the incident shock wave is subsonic for the relatively low incident shock strength tested, these waves move upstream in a direction opposite to that in which the incident shock is moving, the front of the wave being an acoustic pulse travelling at the local sonic velocity. They carry a 'message' to the approaching flow that an expansion has just occurred. Whenever the shock expands in the remainder of the system, further expansion waves will be generated in a similar manner.

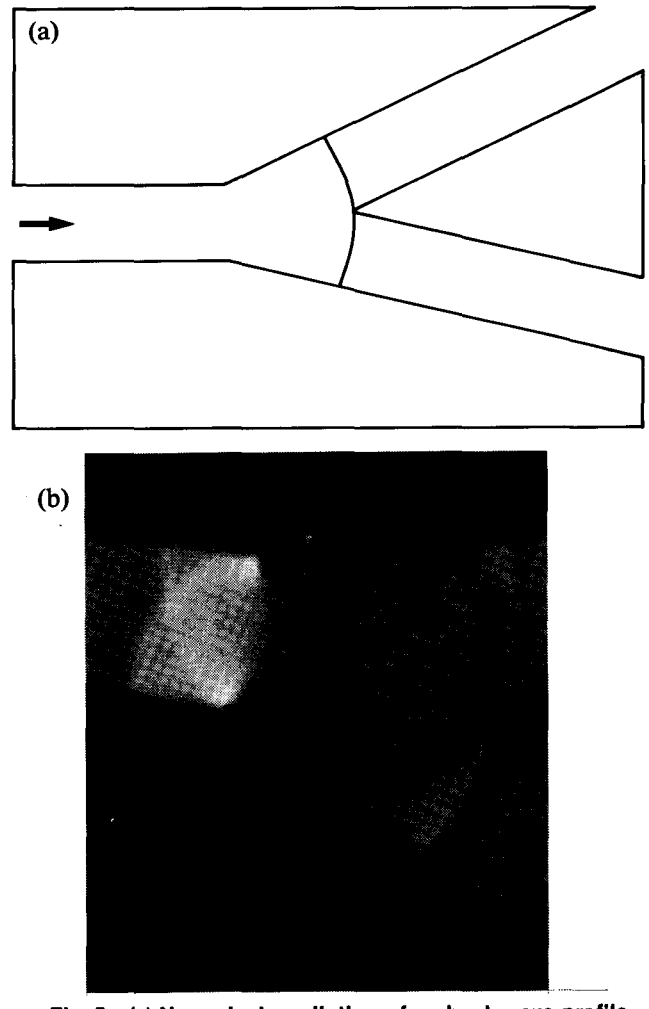

Fig. 5—(a) Numerical prediction of a shock-wave profile (b) The corresponding schlieren photograph

In Fig. 6 (30 μs later), the shock has expanded into the first junction. The oval-shaped wave is the reflection off the apex. This reflection continues to grow in size until it is itself reflected off the side walls, forming secondary and tertiary reflections that weaken and eventually dissipate in the turbulence of the system.

Some 60 μs later, as shown in Fig. 7, the shock moves into the second junction. A strong vortex, visible as a dark mass of rotating fluid, forms as the shock negotiates the obtuse corner. An expansion wave is again generated, moving in a direction opposite to that of the incident shock. The shock wave reflecting off the far wall of this junction appears white in the photograph since the density gradient is in the opposite direction to that of the incident wave.

At this stage of the flow, an interesting feature develops in the inlet junction attached to the lower corner of the entrance duct and inclined to the axis of this duct at approximately 20°. This strong density gradient is nearly stationary with respect to the junction. Furthermore, a photograph taken 32 μs later, Fig. 8, shows two of these features, lying parallel to each other and still embedded in the inlet junction. While practically all the other features visible in the schlieren photographs can be explained in terms of reflections, expansions, or vortices, these features require further study. At this stage of the

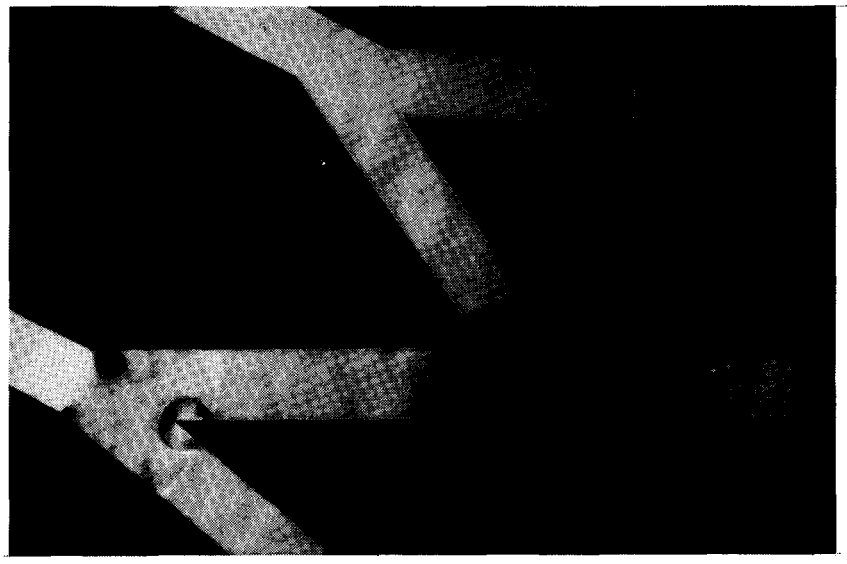

Fig. 6—The initial wave reflection in the first junction

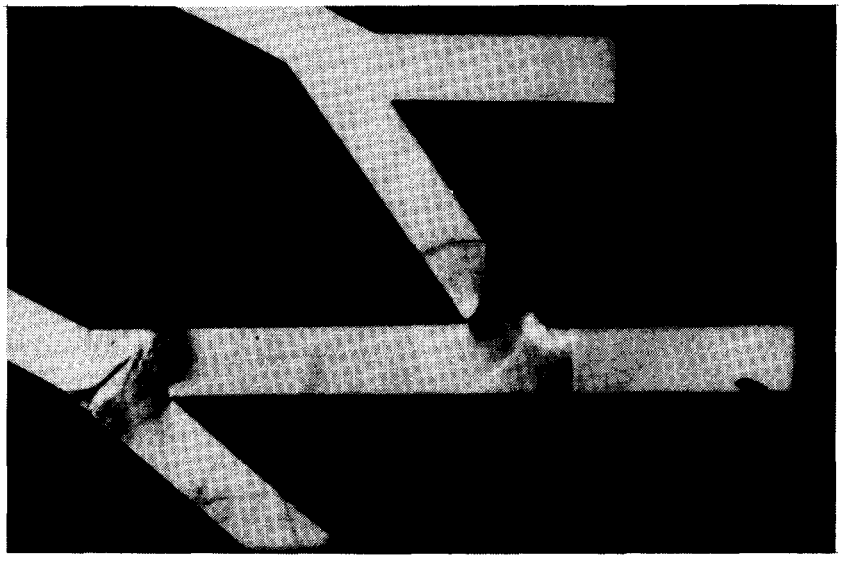

Fig. 7—Wave interactions in the second junction

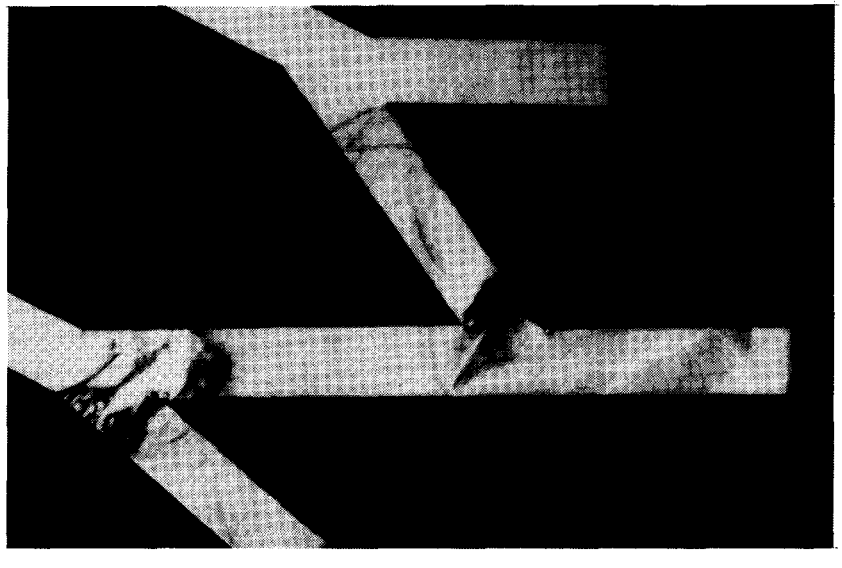

Fig. 8—Flow features in the entrance region

process, the flow separation at the sharp corners of the entrance junction has developed into a turbulent patch spanning the full width of the duct. This turbulence quickly grows in magnitude until it engulfs the whole system, making individual shocks very difficult to distinguish.

Fig. 9 shows a trace from the pressure transducer located in the lower branch of the first junction. The first pressure rise is due to the passage of the initial shock wave. This is followed by a short time delay as this wave travels to the end of the duct, is reflected, and propagates back over the transducer, giving a further pressure increase. This reflected wave results in a pressure on the back wall that is equivalent to twice that behind the incident shock, which has itself approximately doubled the pressure ahead of it. The strength of the reflected wave is determined by the boundary condition that the flow at the end face of the duct must have zero velocity. Since this reflected wave must bring flow at nearly 100°C and moving at over 600 km/h to rest, the pressure ratio across it is understandably high.

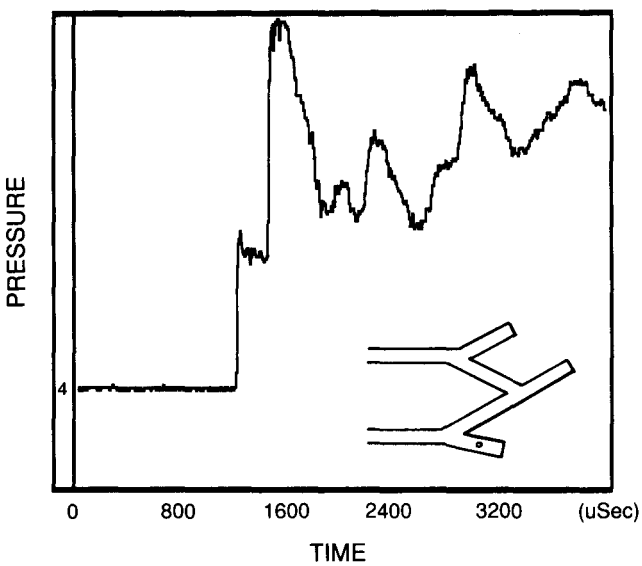

Fig. 9—Particular pressure characteristics of reflection

The subsequent fluctuations of pressure can be correlated with the wave patterns in the schlieren photographs. The general trend of pressure is, however, of more significance. Fig. 10 shows the results obtained from three of the transducers, superimposed. The transducer location within the ducts is not important, since all the transducers, over the long time base represented in this trace, show the same general behaviour. It is noted that by about 3,6 ms after the shock wave first enters the system, the average pressure inside the duct system has risen to approximately double the pressure behind the original shock. The interaction of all the waves in all the branches of the test section thus reaches a general maximum after the incident shock first arrives, producing the general doubling of pressure over that behind the incident wave. This high-pressure source can then act to drive a shock down the exit leg of the duct.

The basis of the numerical model, as presented earlier, involves a major explicit approximation—namely, the neglect of all reflected waves. Judged from the schlieren photographs, this would seem to be an invalid approximation, yet it depends on the energy density of these reflected waves in comparison with that of the incident shock. The results obtained from the program generally compared well with the shock-wave Mach numbers derived from the pressure traces. Fig. 11 shows the numerical

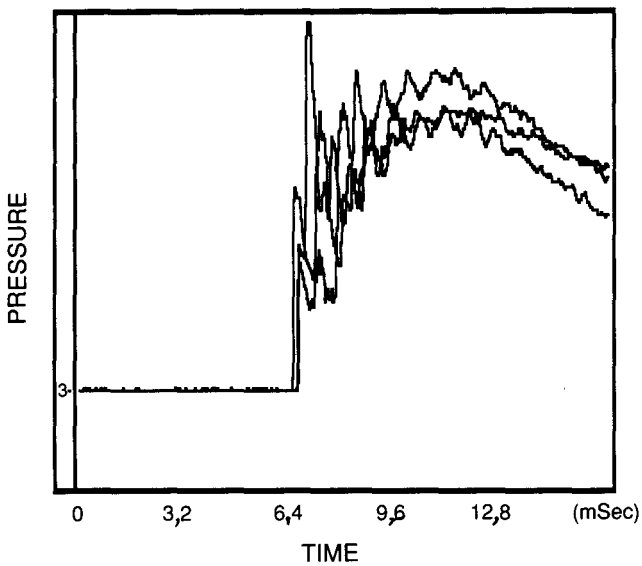

Fig. 10—General pressure characteristics of the system

estimate of the Mach number in the lower branch of the first junction compared with the experimental value, both plotted against the inlet Mach number to the system. The largest recorded error in this branch was 4,8 per cent. In that case, the error is a smoothly increasing function of Mach number and could be extracted to generate an empirical factor, itself a function of Mach number, which could be subtracted from further estimates to produce a modified estimate with negligible error. Whether this would apply over a wider range of incident Mach numbers would need to be established. Calculations for the second junction (both branches) predicted the measured values to within 10 per cent. This lower accuracy is due to the curvature of the wave incident on the junction, whereas the analysis assumes a plane wave. Since the output shock strength for one limb of the duct acts as an input to the next junction, the errors would tend to accumulate unless there was sufficient distance between junctions to ensure the development of a plane wave.

Fig. 12 is a numerical estimate of the time delay, along with the measured value, both again plotted against the inlet Mach number to the system. The time delay, mentioned earlier, was the time taken for a shock to pass over a transducer in a closed duct, reflect off the end-wall, and return as a reflected wave. This particular result produced a maximum recorded error of only 2,4 per cent. Typical errors (i.e. the difference between the measured and estimated results) were generally in the range 2 to 6 per cent. The measured and numerically estimated results follow the same general trend, indicating that the approximate theoretical model is of value. While the results presented here were obtained on a small laboratory-scale rig, the numerical procedure can be applied to any branched duct system for estimates of shock strengths. Numerical models are currently under development that will predict fuller details of the whole flow field.

In the original investigation, it was noted that substantial blast effects were evident in the return airway, parallel to the haulage in which the explosion had occurred. It is thus of interest to establish the strength and behaviour of

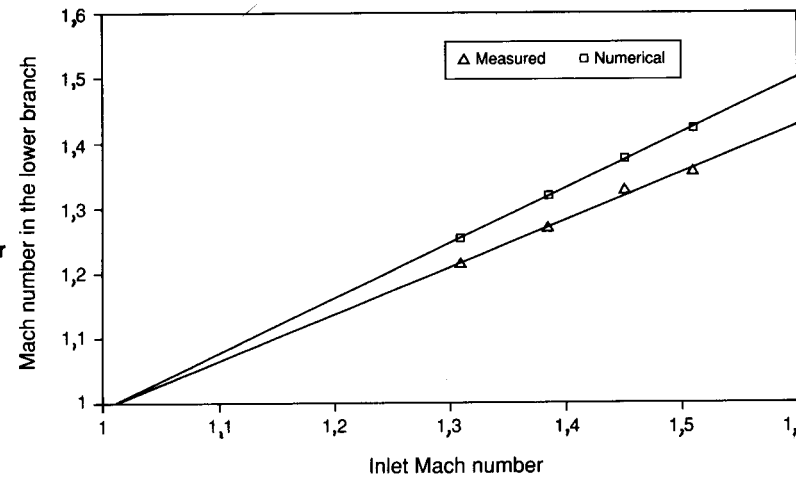

Fig. 11—Numerical estimate of the Mach number

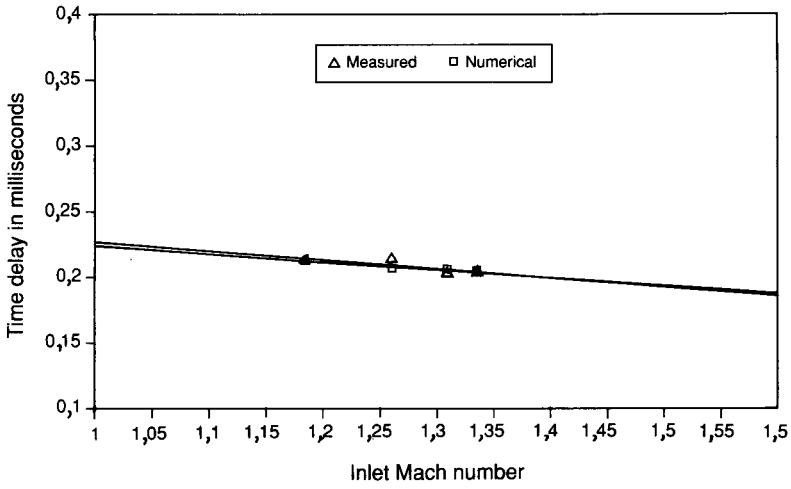

Fig. 12—Numerical estimate of the time delay

the waves that are fed into this tunnel from the development end. In order to investigate this in the laboratory, an extension tube, 1 m in length, was added to the exhaust outlet of the test section. This tube had the same cross-section and wall roughness as the inlet tube. From the schlieren photographs given previously, it is evident that a series of waves will pass into this duct from the test section. Eighteen pressure transducer ports were fitted along the length of this tube in order to track the motion of these waves.

Fig. 13 shows the pressure traces from the six central transducers for a test with an inlet Mach number of 1,6. The traces are arbitrarily separated on the pressure axis for clarity, with the record for the transducer closest to the test section at the top. Three distinct pressure jumps are noted on this trace that identify three distinct shock waves emerging from the test section, the second wave being the strongest. It should be noted that the absolute magnitudes of these jumps should not be compared directly between traces because of the differing transducer calibrations.

The time intervals between the waves on successive traces decrease for transducer positions further from the test section, i.e. the waves are overtaking each other. The first shock wave emerging from the test section is overtaken by the second at the transducer position corresponding to the second-lowest trace on Fig. 13, thereby resulting in a stronger leading wave. This overtaking

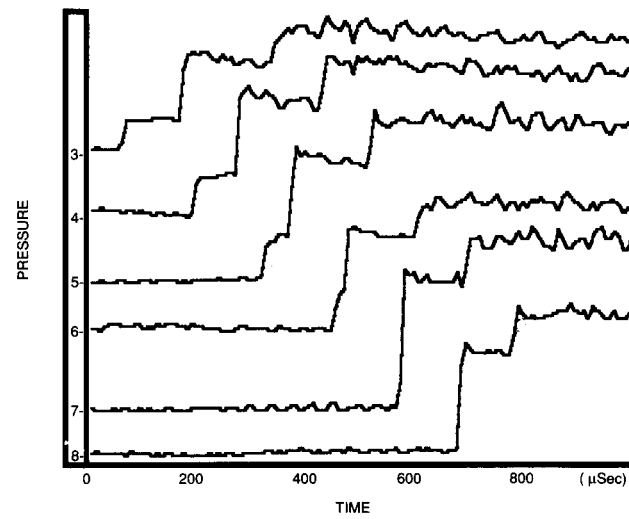

Fig. 13—Pressure distributions in the outlet duct

phenomenon is readily explained. The region between the two waves is reasonably uniform, and a shock wave has the property that the flow into it relative to the wave is supersonic, and the outflow is subsonic. Thus, the second wave moves supersonically with respect to the gas ahead of it, which is itself subsonic with respect to the second wave. The two waves must thus eventually merge.

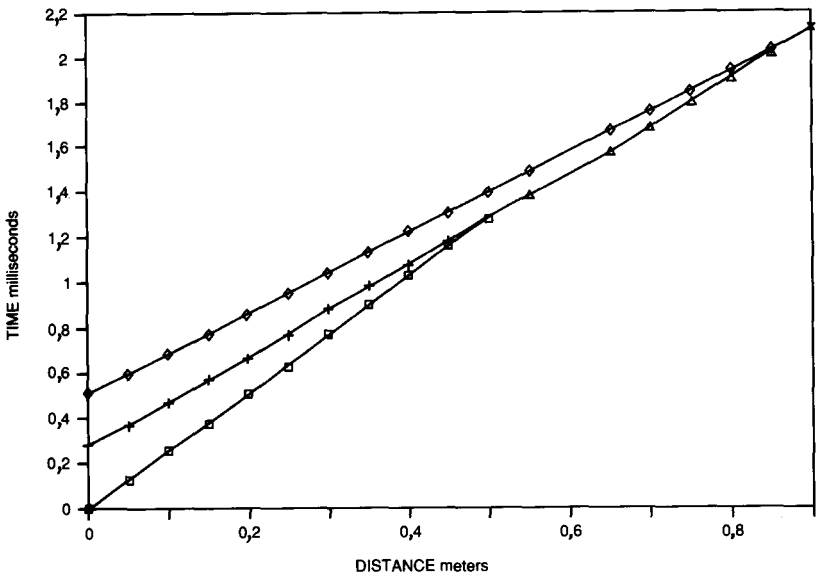

Fig. 14—Wave diagram for the outlet duct

Fig. 14 is a wave diagram (or x, t plot) of the wave motion in the outlet duct. All three of the shock waves have merged into a single wave before the end of the duct is reached. It is noted that the locus of the waves on the wave diagram are nearly linear, and the waves thus propagate at approximately constant velocity. These velocities can thus be determined from the slope of the lines, from which the Mach numbers, and hence temperatures and pressures, can be calculated. For the case shown, the Mach number at the inlet to the test section was 1,6, corresponding to a pressure ratio of 2,82. The first shock emerging from the test section had a Mach number of 1,14 and a pressure ratio of 1,35, whereas the final merged wave was moving at Mach 1,41 and a pressure ratio of 2,15. The complex tunnel system between the inlet and the outlet ducts thus had a net effect of reducing the peak pressure behind the blast by only 24 per cent for the case tested. The effects of different inlet wave strengths and other geometries have not been tested, and it is not inconceivable, if area changes occur, that wave amplification may result.

Conclusion

A model study of gas-dynamic effects resulting from a shock wave propagating through a complex system of branched ducts showed a number of interesting features.

- The flow is complex, but can be understood when the individual waves are tracked on a series of individual schlieren photographs taken at short time intervals.
- A first approximation of the strength of the waves propagating in the various limbs can be made by use of simple numerical procedures.
- Reflection boundaries in the tunnel complex result in a general increase of pressure in the cavity, which results in the transmission of shock-induced high pressures to the connecting tunnels.
- Waves emerging into adjacent tunnels tend to become plane and overtake each other, thereby resulting in stronger waves further along the tunnel.

The study explored only the wave behaviour in a single tunnel geometry, and over a limited range of inlet shock-wave Mach numbers. The effects of wall roughness on wave attenuation were not explored, nor were the effects of the initial wave-pressure profile. A substantially extended series of tests would be needed in order to address these factors.

References

1. SMOLENIEC, S. Report on blast wave effects on the site of accident at President Steyn Gold Mine on 24-12-1959. Johannesburg, University of the Witwatersrand, 1962.
2. HEILIG, W.H. Propagation of shock waves in various branched ducts. *Proceedings of the Tenth International Shock Tube Symposium.* Kyoto, 1975.
3. WHITHAM, G.B. A new approach to problems of shock dynamics. *J. Fluid Mech.*, vol. 2. 1957. pp. 145–165.
4. CHESTER, W., and CHISNELL, R.F. The motion of a shock wave in a channel. *J. Fluid Mech.*, vol. 2. 1957. p. 286.
5. SKEWS, B.W. The shape of a diffracting shock wave. *J. Fluid Mech.*, vol. 29, pt 2. 1967. pp. 286–304.